

BIOCHEMISTRY (ISSN: 0006-2960) 53: (31) pp. 5186-5198. (2014)

DOI: 10.1021/bi500553f

Temperature Dependence of Backbone Dynamics in Human Ileal Bile Acid-Binding Protein. Implications for the Mechanism of Ligand Binding

*Gergő Horváth, Orsolya Egyed, and Orsolya Toke**

Institute of Organic Chemistry, Research Centre for Natural Sciences, Hungarian Academy of Sciences, 2 Magyar tudósok körútja, H-1117 Budapest, Hungary

AUTHOR INFORMATION

Corresponding Author

*O. Toke, Ph.D.

Phone: +36-1-382-6575

Fax: +36-1-382-6295

E-mail: toke.orsolya@ttk.mta.hu

Funding Sources

The work was supported by the Hungarian Research Fund OTKA via K 109035 (O.T.).

ABBREVIATIONS

CPMG, Carr-Purcell-Meiboom-Gill; CRBP, cellular retinol binding protein; FABP, fatty acid binding protein; GCA, glycocholic acid; GCDA, glycochenodeoxycholic acid; ITC, isothermal titration calorimetry; I-BABP, ileal bile acid-binding protein; NMR, nuclear magnetic resonance

KEYWORDS: lipid-binding proteins, enterohepatic circulation, bile salts, conformational exchange, protein dynamics, binding cooperativity, site-selectivity, NMR spectroscopy

ABSTRACT

Human ileal bile acid-binding protein (I-BABP), a member of the family of intracellular lipid binding proteins plays a key role in the cellular trafficking and metabolic regulation of bile salts. The protein has two internal and according to a recent study an additional superficial binding site and binds di- and trihydroxy bile salts with positive cooperativity and a high degree of site-selectivity. Previously, in the *apo* form, we have identified an extensive network of conformational fluctuations on the ms time scale, which cease upon ligation. Additionally, ligand binding at room temperature was found to be accompanied by a slight rigidification of ps-ns backbone flexibility. In the current study, temperature-dependent ^{15}N NMR spin relaxation measurements were used to gain more insight into the role of dynamics in human I-BABP – bile salt recognition. According to our analysis, residues sensing a conformational exchange in the *apo* state can be grouped into two clusters with slightly different exchange rates. The entropy-enthalpy compensation observed for both clusters suggests a disorder-order transition between a ground and a sparsely populated higher energy state in the absence of ligands. Analysis of the faster, ps-ns motion of $^{15}\text{N}-^1\text{H}$ bond vectors indicates an unusual nonlinear temperature-dependence for both ligation states. Intriguingly, while bile salt binding results in a more uniform response to temperature change throughout the protein, the temperature derivative of the generalized order parameter shows different responses to temperature increase for the two forms of the protein in the investigated temperature range. Analysis of both slow and fast motions in human I-BABP indicates largely different energy landscapes for the *apo* and *holo* states suggesting that optimization of binding interactions might be achieved by altering the dynamic behavior of specific segments in the protein.

Human ileal bile acid binding protein (I-BABP), expressed in the absorptive enterocytes of the distal small intestine has a key role in the enterohepatic circulation of bile salts.¹ In addition to aiding the absorption of lipidlike compounds in the human body², bile salts (Figure 1) are also known as signal molecules, which play important roles in the regulation of metabolic processes. In particular, by binding to the nuclear farnesoid X receptor α (FXR)³ they provide a negative feedback mechanism for their own synthesis thereby contributing to the maintenance of whole-body cholesterol homeostasis. In addition, by the activation of various mitogen-activated protein kinase pathways and the interaction with the G-protein-coupled receptor TGR5, they participate in the regulation of triglyceride, energy, and glucose metabolism.⁴

Within the family of intracellular lipid-binding proteins (iLBPs), a group of small 14-15 kDa polypeptide chains which are known to facilitate the cellular trafficking of lipidlike compounds (e.g. fatty acids, retinoids, bile salts)⁵⁻⁶, human I-BABP is a protein with unique properties. Unlike most of the other members of the family, I-BABP has two internal⁷ and according to a recent study an additional superficial⁸ binding site and depending on the hydroxylation pattern of the bound bile salts exhibits a moderate-to-high level of positive binding cooperativity.⁹ In addition, the protein has been found to show a high degree of site-selectivity in its interactions with glycocholate (GCA) and glycochenodeoxycholate (GCDA), the two most abundant bile salts in humans.¹⁰ As a result, while in homotypic complexes di- and trihydroxy bile salts occupy both internal binding sites, in the heterotypic complex of I-BABP:GCDA:GCA, they displace each other and selectively occupy site 1 and site 2, respectively. An analogous site-selectivity for di- and trihydroxy bile salts has been reported for the disulfide-containing polymorph (T91C) of chicken liver bile acid-binding protein (cl-BABP).¹¹ Intriguingly, while in human I-BABP site-selectivity is thought to arise as a result of

localized enthalpic effects, NMR relaxation measurements in cl-BABP suggests a possible connection with differences in protein flexibility.

Although no X-ray structure of the 14.2 kDa I-BABP is available yet, NMR spectroscopic investigation of the *apo*¹² and the *holo*¹²⁻¹⁴ protein has revealed a topology characteristic of iLBPs.⁵ The dominant feature of this is a β-clam comprised of two antiparallel five-stranded β-sheets and a helix-turn-helix motif. A cavity of ~1000 Å³ located inside of the β-clam hosts two internal binding sites. Additionally, the existence of a third binding site on the protein exterior was proposed recently based on docking calculations and molecular dynamics simulations.⁸ The mechanism of ligand entry and exit is not fully understood in I-BABP. In other members of the iLBP family with the same topology, such as fatty acid binding proteins (FABPs), the helical cap region disordered in the *apo* state is thought to be the main regulator of ligand association/dissociation.¹⁵⁻¹⁷ Specifically, according to the dynamic portal hypothesis, ligand binding is accompanied by an ordering of the helical cap and the stabilization of the closed state of the protein. Unlike in FABPs, in human I-BABP the two α-helices are well defined in both ligation states and there is no sign of intense motion¹⁸, raising the possibility of alternative entry/exit mechanisms as it has been suggested for other analogues.¹⁹⁻²²

The internal binding cavity of I-BABP is unusual in the sense that it contains a large number of hydrophilic side chains that are involved in extensive networks of salt bridges and hydrogen bonds. In fact, NMR spectroscopic and mutagenesis studies have identified two hydrogen-bonding networks as a likely way of energetic communication between the two binding sites.²³ More recently, in an NMR relaxation study of the protein backbone, we have detected a μs-ms fluctuation in the unligated protein affecting several β-strands and the C-D loop, a motion which ceases upon ligation.¹⁸ Our NMR dynamic measurements with previously

obtained kinetic data²⁴ suggest that conformational fluctuations have an important role in bile salt-human I-BABP recognition. A conformational transition on a similar time scale has been proposed earlier for several other members of the iLBP family, including the intestinal FABP¹⁶, cellular retinol binding proteins (CRBP I and II)¹⁷, and cl-BABP¹⁹, indicating that it might be a general way of mediating ligand binding in the protein family.²²

To improve our understanding of the role of dynamics in human I-BABP-bile salt recognition, we report here a characterization of the temperature dependence of slow (microsecond to millisecond) and fast (picosecond to nanosecond) backbone motions in the protein through the use of ¹⁵N NMR spin-relaxation analysis. Atomic scale dynamic parameters obtained from the NMR measurements are discussed in the context of previously obtained macroscopic thermodynamic and kinetic data.

MATERIALS AND METHODS

Sample Preparation. The methods used for the expression and purification of ¹⁵N, ¹³C/¹⁵N, and ²H/¹⁵N-labeled human I-BABP used in the experiments are detailed elsewhere.¹⁸ Protein was dialyzed into a buffer containing 20 mM potassium phosphate, 50 mM KCl, and 0.05 % NaN₃ at pH =6.3. Protein concentration was 1 mM in all experiments. In the case of the *holo* sample, protein was complexed with an equimolar mixture of GCA and GCDA at a molar ratio of I-BABP:GCDA:GCA=1.0:1.5:1.5, ensuring that over 99.9% of the protein was in its bound state.⁹

NMR Data Collection. Multidimensional NMR experiments were carried out at 283, 287, 291, 298, and 313 K on 600 MHz Varian NMR SYSTEM™ spectrometer equipped with a 5-mm indirect detection triple ¹H/¹³C/¹⁵N resonance z-axis gradient probe. The backbone resonance assignment of *apo* human I-BABP and that of the heterotypic doubly-ligated complex

at 298 K has been published earlier.¹⁸ To obtain the amide ¹H and ¹⁵N assignment at the newly investigated temperatures, the 298 K assignment has been transferred to the corresponding spectra and confirmed by 3D gradient enhanced HNCACB²⁵⁻²⁷ and/or CBCACONNH²⁸ experiments performed on uniformly [U-¹³C/¹⁵N]-enriched human I-BABP. Spectral processing, computer-assisted spin-system analysis, and resonance assignment was carried out using Felix 2004 (Accelrys, Inc.). The ¹⁵N T₁, T₂, and steady-state {¹H}-¹⁵N NOE measurements²⁹⁻³¹ were collected on U-[¹⁵N]-enriched *apo* and *holo* human I-BABP at 283, 291, 298, and 313 K. Backbone amide ¹⁵N T₁ values were measured from two series of eight spectra (24 transients, interscan delay of 1.5 s) at each temperature with the following relaxation delay times T = 20, 100, 190, 290, 390, 530, 670, and 830 ms, and T = 20, 50, 100, 170, 240, 340, 480, and 630 ms. Amide ¹⁵N T₂ values were obtained similarly: T = 10, 30, 50, 70, 110, 150, and 190 ms, and T = 10, 30, 50, 90, 130, 150, and 170 ms. Steady-state {¹H}-¹⁵N NOE values were obtained in triplicate (32 transients each) by recording spectra with and without (blank) the use of ¹H saturation applied during the last 5 s of a 7 s delay between successive transients. Presaturation was achieved with the use of 120° ¹H pulses applied every 5 ms.³² The RF field strength of the ¹H hard pulse was 11.6 kHz.

Relaxation dispersion data were obtained on [80% ²H, 99% ¹⁵N]-labeled protein at 283, 287, and 291 K, using a relaxation compensated Carr-Purcell-Meiboom-Gill (CPMG) dispersion experiment performed in a constant time manner.³³⁻³⁴ The constant time delay (T_{CP}) was set to 40 ms. Spectra were collected as a series of 20 two-dimensional data sets with CPMG field strengths (v_{CPMG}) of 25, 50, 74, 99, 123, 147, 172, 195, 219, 242, 289, 335, 380, 425, 469, 556, 641, 764, and 883 Hz. A reference spectrum was obtained by omitting the CPMG period in the pulse sequence.³⁵ Spectra (3 s interscan delay, 24 transients) were acquired in duplicate.

Model-Free Analysis. Spectral densities were calculated from the ^{15}N T_1 , T_2 , and steady-state $\{\text{H}\}-^{15}\text{N}$ NOE relaxation parameters according to Abragam.³⁶ Amide N-H bond lengths were assumed to be 1.02 Å and the ^{15}N chemical shift anisotropy was estimated as -172 ppm during the calculation.³⁷ To characterize the spatial restriction of the ^{15}N - ^1H bond vector on the picosecond to nanosecond time scale, the NMR relaxation data were analyzed within the extended model-free formalism.³⁸⁻⁴¹ Motional parameters have been determined using FAST-Modelfree (Facile Analysis and Statistical Testing for Modelfree⁴²), interfaced with Modelfree 4.2⁴³⁻⁴⁴ as detailed elsewhere.¹⁸ To minimize the inconsistencies with a continuous temperature dependence of the order parameter arising from different model selection at different temperatures, if at least at two of the four investigated temperatures FAST-Modelfree chose a more complicated model with two or three parameters, the same model was imposed onto the amide at the two remaining temperatures as well. An initial estimate of the rotational diffusion tensor was calculated from the filtered T_1/T_2 ratios using the programs r2r1_diffusion (http://www.palmer.hs.columbia.edu/software/r2r1_diffusion.html) and pdbinertia (<http://biochemistry.hs.columbia.edu/labs/palmer/software/pdbinertia.html>). The criteria for inclusion of residues in the diffusion tensor estimate relied on the method by Kay et al.⁴⁵ Coordinates for the *apo* and *holo* form were obtained from PDB files 1O1U¹² and 2MM3¹⁴, respectively.

To relate the NMR-derived motional parameters to macroscopic thermodynamic data, the order parameter, S^2 , obtained from the model-free analysis, was used to calculate a conformational entropy value for the angular fluctuation of individual N-H bond vectors according to⁴⁶⁻⁴⁷

$$S_B = k_B \ln [\pi(3 - (1 + 8S)^{1/2})] \quad (1)$$

in which S_B is the backbone conformational entropy and k_B is the Boltzmann's constant.

The contribution of various sources of entropy change accompanying ligand binding to calorimetrically measurable entropy change is discussed in terms of

$$\Delta S^o = \Delta S_{conf} + \Delta S_{rot-trans} + \Delta S_{hydr} \quad (2)$$

where ΔS_{conf} is the change in conformational entropy of the protein and the ligand, $\Delta S_{rot-trans}$ is the change in the rotational-translational entropy of the system, and ΔS_{hydr} is the entropy change due to the changes in the hydration of the interacting partners.

Relaxation Dispersion Analysis. Contributions to transverse relaxation rates of conformational exchange were analyzed assuming a two-state exchange process using the all-timescales multiple quantum Carver-Richards-Jones formulation⁴⁸ implemented in GUARDD.⁴⁹

RESULTS

Temperature Dependence of Slow Conformational Motions. Representative transverse relaxation dispersions as a function of CPMG field strength as determined for *apo* human I-BABP at 283 K, 287 K, and 291 K are plotted in Figure 2. Dispersion profiles were first individually fit at each temperature assuming a two-state exchange process between a ground and an excited state as described in Materials and Methods. The average individual exchange constants and excited state populations along with the average values of R_{ex} and chemical shift differences between the two exchanging states are listed in Table S1-S3 of the Supporting Information. About one third of the assignable ~115 residues have been found to undergo a conformational exchange with a $R_{ex} > 2$ Hz in the investigated temperature range. Among these, 30 residues showed a measurable R_{ex} at all three temperatures.

Similarly to measurements conducted previously at 298 K¹⁸, residues sensing a millisecond exchange process in the 283-291 K range form an extended dynamic network in *apo* human I-BABP (Figure 3). Fluctuations with the largest values of R_{ex} (10-25 s⁻¹) are detected in the E-F (T73) and G-H (V91, N96, H98) regions in the C-terminal half of the protein. These four residues are part of the two longest continuous segments (E69-V83 and L90-E102) in the protein exhibiting a R_{ex} . Additionally, a near continuous stretch of eleven (H52-K62) and six (K35-V40) residues show evidence of a millisecond motion in the C-D loop throughout beta-strand D as well as in beta-strand B together with a preceding linker to helix-II. While the C-D region and residue K35 showed a measurable R_{ex} at 298 K as well, the slow motion in beta-strand B has not been detected before. Furthermore, evidence of a slow conformational exchange is indicated near the N-terminus on beta-strand A (K5, E7, E11) continuing (N13) in helix-I (D15, E16, F17) as well as toward the C-terminus of the protein in segments of beta-strands I (V109, E110, T113) and J (Y119, R121, V122, K124).

According to the individual fit of the dispersion profiles obtained in the 283-291 K temperature range, backbone amides appear to be clustered into two main groups (Figure 3) indicating the presence of two slightly different exchange processes in the system. Most of the residues in the E-F and G-H regions have been found to undergo an exchange process with values of k_{ex} averaging around 769 ± 59 s⁻¹ (283 K), 1088 ± 195 s⁻¹ (287 K), and 1401 ± 141 s⁻¹ (291 K), whereas the rest of the amides exhibiting a R_{ex} throughout the protein appear to display a slower average k_{ex} of 265 ± 82 s⁻¹ (283 K), 658 ± 45 s⁻¹ (287 K), and 878 ± 86 s⁻¹ (291 K). The similarity of the exchange constants obtained for the amides within each cluster justifies a global fit with a single rate constant for each. As adequate fits of the dispersion profiles were achieved with the assumption of a two-state exchange, two separate A↔B and A↔C processes have been

considered. Parameters determined from the global fit analysis of the two exchange processes are listed in Table 1. The slightly higher excited state population determined for cluster I indicates a more pronounced presence of the conformational equilibrium involving the C-terminal half of the protein. The temperature dependence of $\ln(k_{BA}/k_{AB})$ and $\ln(k_{CA}/k_{AC})$ has been used to calculate $\Delta H = 7.0 \pm 1.6$ kcal mol⁻¹ and 4.2 ± 0.1 kcal mol⁻¹ as well as $\Delta S = 17.8 \pm 5.4$ cal mol⁻¹ K⁻¹ and 6.9 ± 0.3 cal mol⁻¹ K⁻¹ for the A to B and A to C transition, respectively, showing a typical entropy-enthalpy compensation characteristic of an order-disorder transition for both clusters. The Gibbs free energies are near 2 kcal mol⁻¹ in the investigated temperature range for both transitions. In light of the two clusters of amides observed in the 283-291 K temperature range, the previously collected data at 298 K¹⁸ was revisited. Although forcing the amides into their corresponding cluster was possible, the resulting values of k_{ex} were nearly the same for both groups (3260 ± 560 s⁻¹ and 2900 ± 400 s⁻¹ for cluster I and II, respectively). The temperature dependence of the forward and reverse rate constants is depicted in Figure 4. Based upon conventional transition state theory, the energy barrier for the A to B and A to C process is estimated to be 19 kcal mol⁻¹ and 26 kcal mol⁻¹, respectively.

The chemical shift differences found for individual ¹⁵N spins mapped to the ribbon diagram of the mean coordinates of *apo* human I-BABP (PDB entry 1O1U¹²) at 287 K are shown in Figure 3B. Similar distribution and amplitude of $\Delta\delta$ have been obtained at 283 K and 291 K. The differences were in general less than 4 ppm, with the largest $\Delta\delta$ values (>1.5 ppm) detected for residues located in the E/F and G/H turns as well as on beta-strand H.

In contrast to the *apo* protein, in the doubly-ligated state about 95% of the relaxation dispersion profiles remain flat in the investigated 283-291 K temperature range. Representative examples of relaxation dispersion profiles for the two ligation states are depicted in Figure S1 of

the Supplementary Information. Ceasing of conformational motion upon ligand binding is widespread in all regions showing an exchange in the *apo* state. This agrees well with our previous observation at higher temperature¹⁸ and indicates that the millisecond conformational motion giving rise to R_{ex} in *apo* human I-BABP is absent in the doubly-ligated form in the entire 283-298 K temperature range.

Temperature Dependence of Fast Protein Motions. Because of their strong effect on entropy, motions on the picosecond to nanosecond timescale have high biological importance.⁵⁰ To characterize the temperature dependence of ps-ns dynamics in the *apo* and *holo* forms of human I-BABP, ¹⁵N T₁, T₂ relaxation and steady-state {¹H}-¹⁵N NOE measurements were performed at 283, 291, 298, and 313 K, and subjected to model-free analysis. For the *apo* protein, ¹⁵N relaxation parameters could reliably be determined for 117, 115, 112, and 103 backbone amide positions of the 126 nonproline residues at 283, 291, 298, and 313 K, respectively. For the *holo* state, 115 (283 K), 116 (291 K), 112 (298 K), and 107 (313 K) residues were included in the analysis. Resonances showing severe overlap and those of low intensity were excluded from the study at each temperature. The average values of ¹⁵N T₁, T₂, and {¹H}-¹⁵N NOE for the two protein states together with the mean values of the generalized order parameters (S^2) are given in Table 2. Generalized order parameters were determined for each of the resonances that could be reliably fit to models 1-5. Although at 283 K and 291 K the majority of the amides could be fit by the simplest model-free formalism using S^2 alone (model 1), substantially more residues required an apparent conformational exchange term (models 3 and 4) to fit their relaxation parameters than previously observed at 298 K.¹⁸ For instance, in the *apo* protein, the number of residues with $R_{ex} > 0$ increased from 11 to 22 to 30 as the temperature was decreased from 298 to 291 to 283 K. A similar tendency was found for the *holo* protein. In

the *apo* protein, the position of the amides exhibiting a conformational exchange according to the model-free analysis generally fell into the regions exhibiting a nonflat dispersion profile in CPMG relaxation dispersion experiments. In the *holo* protein, as dispersion profiles remained almost exclusively flat, no such agreement was found. We should note though that by model-free analysis, only about 20-30% of the affected residues showed a R_{ex} exceeding 2 Hz in both states of the protein and less than 10% could be associated with a $R_{ex} > 5$ Hz. Regarding fast internal motions between 283-298 K, about 20-25% (10-15%) of the assignable ~115 residues required the inclusion of an effective correlation time of τ_e (models 2, 4, and 5) in the *apo* (*holo*) protein and about one third of the affected ones had to be fit by the two-time scale spectral density function (model 5). At 313 K, while the *holo* form behaved according to the description above, in the *apo* state a substantially larger number of backbone amides had to be fit with a two- or three-parameter model.

To relate the generalized order parameters determined from the model-free analysis to the density of thermally accessible states and local conformational heat capacities of a specific amide bond vector along the sequence, the temperature dependence of S^2 was analyzed. To minimize the inconsistencies with a continuous temperature dependence of S^2 and S_B (eq 1) arising from different model selection at different temperatures, if at least at two of the four investigated temperatures FAST Modelfree chose a more complicated model with two or three parameters, the same model was imposed onto the amide at the two remaining temperatures as well. This affected about 30% of the residues in both protein states and resulted in the same motional model across the entire temperature range for nearly 90% of the assignable residues.

Figure 5 shows the temperature dependence of 1-S for a few representative backbone amides located in various parts and various secondary structure elements of the protein in *apo*

and *holo* human I-BABP. Surprisingly, for the vast majority of the residues, the temperature dependence of 1-S appears to be nonlinear indicating ranges of temperature in which the flexibility of amides decreases rather than increases with increasing temperature. In the case of the *apo* protein, the most general behavior is exemplified by K19 (α -helix) and Y119 (β -sheet). It includes a more or less steady increase of flexibility with increasing temperature in the range of 280-300 K followed by a leveling off or a slight decrease. Intriguingly, the reverse is observed for many of the amides in the *holo* state. Specifically, as the temperature rises from 283 K to 291 K to 298 K, a slight decrease in flexibility is detected in the doubly-ligated form followed by an increase in 1-S above 300 K. While for most of the residues fitting of the temperature dependence of 1-S requires a polynom, for about 15% of the amides it maintains a (near) linearity. Most often this occurs in linker or loop regions (e. g. V65, *apo*; M74, *holo*), but as exemplified in the *apo* state by A31 located in the middle of helix-II, occasionally within well-defined segments as well. There is also a fraction of amides for which in the *apo* form a dramatic increase in flexibility occurs above 300 K. This again is mostly observed in loop regions (e.g. M74), with the exception of two residues in beta-strand E (E68, N70). Upon ligand binding, the sharp increase in 1-S above 300 K disappears in most cases.

Figure 6 depicts the value of S^2 mapped on the backbone trace for *apo* and *holo* human I-BABP at the four investigated temperatures as obtained using the imposed model selection protocol as described above. The mean values of S^2 at each temperature are listed in Table 2. In general, the imposed model selection protocol resulted in a slightly smaller mean S^2 than fast model-free but the differences between the complexed and uncomplexed states are nearly the same using both protocols. According to the mean values of S^2 , temperature change in the investigated region of 283-313 K has a somewhat larger effect on the backbone flexibility of *apo*

I-BABP than that of the complexed form, suggesting that in overall, bile salt binding is accompanied by a reduction in the thermally accessible states for the protein backbone. According to both the mean values of S^2 (Table 2) and individual order parameters along the amino acid sequence (Figure 7), ligand binding has a temperature dependent effect on the amplitude of ps-ns motion of backbone amides. This is most clearly seen between the 283 K and the 298 K data. While at 283 K the S^2 of most of the individual backbone amides in the *apo* state is exceeding the values of S^2 detected in the *holo* form, at 298 K it is the other way around. At 313 K, a slight decrease in S^2 occurs upon ligation throughout the protein with the exception of specific regions, where bile salt binding is accompanied by a dramatic decrease in flexibility. The outliers shown in Figure 6 and 7 are located in loop regions or at the termini of secondary structure elements. The largest number of amides with $S^2 < 0.75$ occurs at 313 K in the *apo* state.

Grouping of the temperature dependence of 1-S by secondary structure elements reveals further details about the ligation-induced changes in backbone flexibility. The variation in $d(1-S)/dT$ within each 2° element is depicted in Figure 8 for *apo* and *holo* human I-BABP at three different temperatures as determined by fitting of 1-S vs. T and calculation of the corresponding slope at each specific temperature for individual backbone amides. The box chart form used in Figure 8 allows a simultaneous representation of the median value, the variability, as well as the asymmetry of $d(1-S)/dT$ values in a given structural element. As depicted in Figure 8, at low temperature (near 283 K), while in the *apo* form of the protein the slope of 1-S vs. T is positive, upon ligation it changes its sign throughout the protein. For some of the regions (β_A , β_B , β_C , β_D , β_I , β_J), the absolute value of the slope becomes smaller indicating a less steep temperature dependence. This can be interpreted as a reduction in the thermally accessible states and a

reduced local heat capacity for the given segment. It is worth noting that in some segments of the protein while the slope changes its sign upon bile salt binding, in absolute value it remains the same (α -I, α -II, β_F , β_G , β_H). Moreover, there is one beta-strand (β_E) in which according to the mean value of the slope, the temperature dependence becomes steeper upon ligand binding. It is also noticeable that as a result of complex formation, the spread of $d(1-S)/dT$ within secondary structure elements becomes smaller throughout the entire sequence near 283 K, indicating a more uniform response to temperature in the presence of ligands. At higher temperatures, in particular near 313 K, $d(1-S)/dT$ becomes smaller and negative for most regions in the *apo* protein with the exception of α -II and β_E . For these two segments, the mean value of the slope stays positive and fairly large accompanied by a large variability in the values of $d(1-S)/dT$ among individual backbone amides. Upon ligation, their spread becomes smaller and comparable to the rest of the structural elements.

DISCUSSION

For a thorough understanding of protein function and the ability to modulate binding interactions, the intimate relation of protein structure and dynamics needs to be considered. Human I-BABP is a small but challenging system with two binding sites exhibiting positive cooperativity and site-selectivity in its interactions with structurally diverse bile salts. To improve our understanding of the role of flexibility in human I-BABP function, we used ^{15}N NMR spin relaxation techniques to characterize the temperature dependence of internal motions occurring in the free and doubly-ligated forms on the $\mu\text{s-ms}$ and ps-ns timescales.

The two clusters of residues found to undergo a millisecond time scale conformational fluctuation with slightly different exchange rates involve extensive regions of *apo* human

I-BABP and provide a dynamic connection between distant sites. The ‘faster’ cluster comprises two main continuous segments of residues in the C-terminal half of the protein, whereas the ‘slower’ cluster involves the helical region, the proximate C-D loop, and two beta-strands in the N-terminal half (Figure 3). As approaching room temperature, the exchange rate of the ‘slow’ cluster catches up with the ‘faster’ one (Figure 4) merging into a single network of fluctuation with a k_{ex} of ~ 2000 - 3000 s^{-1} . This matches the time scale of an initial unimolecular kinetic step in the binding scheme proposed previously in a stopped-flow kinetic analysis of human I-BABP – bile salt interaction.²⁴

Many of the residues implicated in either of the two clusters in *apo* human I-BABP exhibit a significant chemical shift change upon bile salt binding.¹⁸ The most affected region appears to be the G-H and E-F regions in both respects. Moreover, in some regions of the protein, particularly those located farther away from the bound bile salts in the *holo* form, thus not subjected to direct ligand effects, there is a fairly good agreement between dynamic chemical shift differences derived from ^{15}N relaxation dispersion experiments and backbone nitrogen chemical shift changes observed upon ligand binding (Figure 9). Thus it seems likely that the ms time scale fluctuations detected by the R_{ex} measurements correspond to conformational transitions between a ground and two low-populated excited states exhibiting conformations reminiscent of that of the *holo* form. A similar correlation has been found by Cagliati and coworkers⁵¹ for cl-BABP, where an extensive network of conformational fluctuation between a ground and a *holo*-like excited state conformation has been proposed to be mediating the access of ligands for the binding cavity in the *apo* form. Interestingly, in other members of the iLBP family, such as FABPs and CRBPs, primarily the helical cap region and the nearby C-D loop have been associated with the regulation of ligand entry by both stopped-flow fluorescence¹⁶ and

NMR relaxation^{15, 17} measurements. Another study of cl-BABP has lead to an extension of the previously proposed ‘dynamic portal hypothesis’ toward a model in which ligands enter through a flexible region consisting of not only the helical cap and the C-D loop but also the E-F region¹⁹. Yet another investigation of the porcine I-BABP analogue has suggested the existence of a second portal for ligand entry involving the G-H region.²⁰ Our temperature-dependent R_{ex} measurements support a conformational selection model of ligand binding in human I-BABP with the involvement of nearly all of the secondary structure elements providing a dynamic communication network between distant regions. While in FABPs the regions involved in conformational exchange also exhibit an enhanced ps-ns motion¹⁵, in BABPs no such correlation between μ s-ms and ps-ns motions is observed. Intriguingly, the temperature dependence of the forward and reverse rate constants associated with the slow conformational fluctuations in *apo* I-BABP shows an enthalpy-entropy compensation indicative of a disorder-order transition. Accordingly, a more disordered excited state with a population of a few percent must be present in the *apo* form.

Besides a likely role in mediating ligand entry, the slow motion involving the G-H and E-F regions in wild-type and disulfide-bridge containing cl-BABP analogues has also been associated with the site-selectivity of ligand binding.¹¹ Moreover, NMR structural data and molecular dynamics simulations on cl-BABP suggest that conformational flexibility of the G-H region is required for an efficient coupling between the two binding sites.⁵² This view is supported by our stopped-flow kinetic studies of the human analogue indicating a role of a conformational change occurring on the time scale of seconds (thereby being distinct from that of mediating ligand entry) in positive binding cooperativity.²⁴ This raises the possibility that a motion mediating ligand entry in the *apo* protein is transformed into a different timescale-motion

in the ligated form. We note that the recently reported third, superficial binding site in human I-BABP is thought to be involved in an allosteric mechanism of ligand binding and is proposed to have a role in both positive cooperativity and site-selectivity.⁸

Superimposed onto the slow motions are small-amplitude local fluctuations in proteins occurring at room temperature on the picosecond-to-nanosecond time scale. Their analysis provides insight into the density of energy states thermally accessible for a given protein segment which when studied in a temperature-dependent manner can be related to local conformational heat capacities, in particular when comparing different ligation states. In our study of human I-BABP, we have found an unusual, nonlinear temperature-dependence of backbone amide ps-ns flexibility and conformational entropy (eq 1) corresponding to a temperature-dependent heat capacity in the investigated temperature range. Moreover, according to our analysis, the sign of the slope of $1-S$ vs. T changes upon ligand binding corresponding to different responses to temperature increase in the two forms of the protein. Regarding the variability of the temperature response within secondary structure elements, while at low temperature (~ 283 K) there is a decrease in variability upon ligation for the entire sequence, at high temperature (~ 313 K) it occurs only at specific regions (Figure 8). We note that a similar nonlinear temperature dependence of backbone ps-ns flexibility was recently observed for the human growth hormone⁵³ and the glutamine binding protein⁵⁴ based on NMR relaxation data.

The sum of the conformational entropy terms determined for individual residues in the two ligation states by NMR relaxation measurements can be used as an upper estimate^{46-47, 55} of the backbone conformational entropy change associated with ligand binding and can be related to macroscopic thermodynamic parameters. According to a previous calorimetric study by Tochtermann et al.⁹, the total entropy change accompanying the binding of a 1:1 molar mixture of

GCA and GCDA to human I-BABP at 25 °C and conditions similar to the ones we used in our NMR relaxation study is ~ -2.6 cal/(mol K). As for protein-ligand interactions in general, this calorimetrically measurable entropy change arises from different sources (eq 2). Based on theoretical studies of protein folding⁵⁶⁻⁵⁷, the value of backbone conformational entropy change of ΔS_{conf}^{bb} ~ -89 cal/(mol K) determined from our NMR relaxation study at 298 K translates into an overall conformational entropy change of ΔS_{conf} ~ -206 cal/(mol K). By considering rotational-translational entropy changes accompanying ligand binding for protein-ligand interactions of similar size⁵⁸, ΔS_{hydr} of bile salt binding in eq 2 can be approximated as ~254 cal/(mol K). Relying on small molecule thermodynamic transfer data⁵⁹⁻⁶⁰, this corresponds to the release of ~ 200 water molecules, which for a protein with a binding cavity of ~1000 Å³, seems reasonable.⁶¹ Tochtrap et al.⁹ has also performed ITC experiments to characterize the temperature dependence of the binding interaction for the human I-BABP:GCA complex. Although due to the strong positive cooperativity of ligand binding, the enthalpy change of the first binding step at lower temperatures (15 and 20 °C) has a large ambiguity in their study, the overall trend of the total enthalpy change indicates a nonlinear temperature dependence and similar to our findings a temperature dependent heat capacity in the 10-40 °C temperature range.

The decrease in the ps-ns backbone flexibility of *apo* and *holo* human I-BABP with increasing temperature as observed in our NMR relaxation study in specific temperature ranges should be caused by intramolecular interactions that increase in strength by increasing temperature. Furthermore, the near concerted response to temperature throughout the entire protein suggests that interactions forming extensive networks between distant protein regions must be responsible for the unusual behavior. Unlike hydrogen bonds, hydrophobic and electrostatic interactions are known to increase in strength with increasing temperature⁶²⁻⁶³ and

our data suggest that they likely have a major contribution to protein stability in human I-BABP. This is supported by a close inspection of the human I-BABP structure revealing a number of possible salt bridges and extensive networks of hydrophobic contacts between different secondary structure elements (Figure 9 and S2).

In conclusion, the analysis of both slow and fast motions in human I-BABP indicates largely different energy landscapes for the two ligation states suggesting that optimization of binding interactions might be achieved by altering the dynamic behavior of specific segments in the protein. Further experiments such as side-chain relaxation data and mutagenesis studies should shed more light on how different time scale motions are channeled into each other upon fine modulation of the identified dynamic interaction networks in the protein.

Table 1. Kinetic and thermodynamic parameters of conformational exchange in *apo* human I-BABP deduced from ^{15}N backbone relaxation dispersion NMR measurements. Residues were subjected to a global fit analysis in each cluster.

| | 283 K | 287 K | 291 K |
|---------------------------------------|--------------|--------------|--------------|
| <i>cluster I</i> | | | |
| | | | |
| k_{ex} (s^{-1}) | 836±59 | 1049±88 | 1540±120 |
| p_b (%) | 3.1±0.2 | 3.9±0.2 | 4.3±0.2 |
| k_{AB} (s^{-1}) | 26±3 | 41±4 | 66±6 |
| k_{BA} (s^{-1}) | 810±57 | 1008±85 | 1474±115 |
| ΔG_{AB} (kcal/mole) | 1.9±0.1 | 1.8±0.1 | 1.8±0.1 |
| ΔH_{AB} (kcal/mole) | | | 7.0±1.6 |
| ΔS_{AB} (cal/(mole K)) | | | 17.8±5.4 |
| <i>cluster II</i> | | | |
| | | | |
| k_{ex} (s^{-1}) | 294±40 | 705±69 | 883±103 |
| p_c (%) | 1.8±0.2 | 2.0±0.2 | 2.2±0.2 |
| k_{AC} (s^{-1}) | 5.3±0.9 | 14±2 | 19±3 |
| k_{CA} (s^{-1}) | 289±39 | 691±68 | 863±101 |
| ΔG_{AC} (kcal/mole) | 2.3±0.1 | 2.2±0.1 | 2.2±0.1 |
| ΔH_{AC} (kcal/mole) | | | 4.2±0.1 |
| ΔS_{AC} (cal/(mole K)) | | | 6.9±0.3 |

Table 2. Summary of ^{15}N NMR spin-relaxation rates, generalized order parameters, and derived backbone conformation entropy contributions for *apo* human I-BABP and the heterotypic ternary complex of I-BABP:GCDA:GCA (1.0:1.5:1.5).

| | 283 K | 291 K | 298 K | 313 K |
|---|-----------|-----------|-----------|-----------|
| <i>apo</i> | | | | |
| $^{15}\text{N} R_1 (\text{s}^{-1})$ | 1.4±0.2 | 1.6±0.2 | 1.7±0.1 | 2.5±0.6 |
| $^{15}\text{N} R_2 (\text{s}^{-1})$ | 14.0±1.3 | 11.4±1.1 | 9.2±0.8 | 7.4±0.8 |
| $\{\text{H}\} \ ^{15}\text{N}$ NOE | 0.80±0.06 | 0.78±0.06 | 0.79±0.05 | 0.78±0.04 |
| $\tau_m (\text{ns})$ | 9.6 | 8.1 | 6.8 | 5.0 |
| D_{\parallel}/D_{\perp} | 1.2 | 1 | 1.1 | 1.1 |
| S^2 | 0.92±0.07 | 0.89±0.06 | 0.85±0.05 | 0.85±0.05 |
| $S^{2, \text{imposed m.s.}}$ | 0.90±0.08 | 0.87±0.07 | 0.82±0.08 | 0.81±0.15 |
| $S_B^{\text{average}} (\text{J/K})^a$ | -2.5±1.2 | -1.9±0.7 | -1.4±0.6 | -1.5±1.1 |
| $S_B (\text{cal}/(\text{mole}\cdot\text{K}))^a$ | -447±219 | -341±128 | -254±109 | -277±201 |
| <i>holo</i> | | | | |
| $^{15}\text{N} R_1 (\text{s}^{-1})$ | 1.2±0.09 | 1.5±0.1 | 1.8±0.2 | 2.2±0.2 |
| $^{15}\text{N} R_2 (\text{s}^{-1})$ | 13.7±1.1 | 11.6±1.6 | 9.8±1.4 | 7.0±0.7 |
| $\{\text{H}\} \ ^{15}\text{N}$ NOE | 0.80±0.05 | 0.79±0.06 | 0.78±0.05 | 0.82±0.04 |
| $\tau_m (\text{ns})$ | 9.7 | 8.2 | 6.8 | 5.2 |
| D_{\parallel}/D_{\perp} | 0.9 | 0.9 | 1.0 | 1.0 |
| S^2 | 0.87±0.06 | 0.90±0.05 | 0.88±0.06 | 0.87±0.06 |
| $S^{2, \text{imposed m.s.}}$ | 0.87±0.06 | 0.89±0.05 | 0.86±0.09 | 0.84±0.07 |
| $S_B^{\text{average}} (\text{J/K})^a$ | -1.8±0.7 | -2.1±0.7 | -1.9±0.8 | -1.5±0.6 |
| $S_B (\text{cal}/(\text{mole}\cdot\text{K}))^a$ | -336±128 | -376±128 | -343±146 | -270±109 |

^aCalculated using the imposed model selection described in Materials and Methods. Briefly, if at least at two of the four investigated temperatures FAST-Modelfree chose a more complicated model, the same model was imposed onto the amide at the two remaining temperatures as well.

ASSOCIATED CONTENT

Supporting Information. Tables containing the exchange parameters derived from individual fit of the relaxation dispersion curves, generalized order parameters, and contributions to backbone conformational entropy as determined by model-free analysis. Figure showing representative examples of relaxation dispersion profiles for the *apo* and the *holo* protein , figure of salt bridges and hydrophobic contacts in the *holo* protein. This material is available free of charge via the Internet at <http://pubs.acs.org>.

Author Contributions

The manuscript was written through contributions of all authors. All authors have given approval to the final version of the manuscript.

ACKNOWLEDGMENT

The authors are indebted to D. P. Cistola for the plasmid of human I-BABP.

FIGURE CAPTIONS

Fig. 1 General structure of physiologically relevant bile salts. The vast majority of the derivatives of cholic ($R_1, R_2 = OH$), chenodeoxycholic ($R_1=OH, R_2=H$), and deoxycholic ($R_1=H, R_2=OH$) acid in the human body exist in a glycine ($A= -NHCH_2COOH$, 67 %) or taurine ($A=-NHCH_2CH_2SO_3H$, 23 %) conjugated form.

Fig. 2 Two-state conformational exchange model for human I-BABP. Transverse relaxation dispersions of the backbone ^{15}N nuclei of V91 (A) and H52 (B) in *apo* human I-BABP as a function of CPMG B_1 field strength at temperatures of 283, 287, and 291 K. Solid lines correspond to global two-state exchange models with parameters listed in Table 1 for cluster I (A) and cluster II (B).

Fig. 3 Contribution to transverse relaxation from conformational exchange as derived from CPMG relaxation dispersion measurements on *apo* human I-BABP. A) Values of R_{ex} determined assuming two separate two-state global exchange processes corresponding to cluster I (black) and II (grey) at 283 K (circle), 287 K (triangle), and 291 K (star). B) Backbone ^{15}N chemical shift modulations observed at 287 K with parameters listed in Table 1. Differences in chemical shifts ($\Delta\delta_i$) were normalized with respect to their maximum value ($\Delta\delta_{max}$) and mapped on the ribbon representation of the mean structure of the protein (PDB entry 1O1U¹²) in a pink-to-red (cluster I) and yellow-to-orange (cluster II) gradient. Residues exhibiting a flat dispersion profile or with no available data are colored in grey.

Fig. 4 Temperature dependence of conformational exchange in *apo* human I-BABP. Forward (closed) and reverse (open) rate constants of the conformational exchange in cluster I (triangle) and II (circle) obtained from global two-state analysis of relaxation dispersion curves. Linear fit of parameters was obtained using data obtained at 283, 287, and 291 K.

Fig. 5 Examples of ps-ns backbone flexibility as determined from ^{15}N NMR spin relaxation measurements in *apo* human I-BABP (open circles/dashed lines) and the heterotypic doubly-ligated complex of human:I-BABP:GCDA:GCA (closed circles/solid lines). The values of $1-\text{S}$ are shown as a function of temperature for residues located in different secondary structure elements: α -helix (K19 and A31), loop (V65 and M74), and β -sheet (N70 and Y119).

Fig. 6 Temperature dependence of the order parameters for free and doubly-ligated human I-BABP. The values of S^2 are mapped onto the backbone trace of the mean coordinates of *apo* human I-BABP (PDB entry 1O1U¹²) (*top*) and that of the heterotypic I-BABP:GCDA:GCA complex (PDB entry 2MM3¹⁴) (*bottom*) and color coded in a pink-to-blue gradient. Residues exhibiting a $S^2 < 0.75$ are depicted in darker red. Grey represents proline or overlapping residues or those for which S^2 could not be quantified by modelfree-analysis.

Fig. 7 Temperature dependence of the effect of ligation on backbone amide ps-ns flexibility. Differences of the generalized order parameters determined between the heterotypic doubly-ligated complex of I-BABP:GCDA:GCA (1.0:1.5:1.5) and *apo* human I-BABP are shown at 283, 291, 298, and 313 K.

Fig. 8 Temperature response of backbone flexibility by secondary structure elements in *apo* and *holo* human I-BABP. The values of $d(1-S)/dT$ are shown at 286, 298, and 310 K by curve-fitting of $1-S$ vs. T for each residue for which S^2 could be quantified and calculating the derivative at each specific temperature. The variation in $d(1-S)/dT$ within each secondary structure element is depicted in a box-chart representation. The bar and the dot inside the box indicate the median and the mean value of $d(1-S)/dT$, respectively, whereas the ends of the box correspond to the upper and lower quartile of the data. The crosses extending from the box indicate minimum and maximum data values within a given secondary structure element. Elements of secondary structure are listed in order of their occurrence in the protein sequence. The ratio of the number of residues used in the analysis relative to the total number of nonproline residues in a given segment is shown at the bottom of the chart at each temperature. The heights of the charts are scaled according to the scale of the vertical axis.

Fig. 9 Conformational exchange in human I-BABP. A) Correlation between ^{15}N backbone chemical shift differences deduced from relaxation dispersion measurements on *apo* human I-BABP ($\Delta\omega$) and those detected upon binding an equimolar mixture of GCDA and GCA at a molar ratio of 1.0:1.5:1.5 ($\Delta\delta$). B) Residues exhibiting a linear correlation ($R^2=0.98$, slope=1.1) between $\Delta\omega$ and $\Delta\delta$ are indicated in black on the mean structure of *apo* human I-BABP (PDB entry 1O1U¹²).

Fig. 10 Salt bridges (A) and hydrophobic contacts (B) in *apo* human I-BABP.¹² For clarity, only residues involved in contacts between different secondary structure elements are shown in B). Similarly extensive electrostatic and hydrophobic contacts exist in the *holo* state¹³⁻¹⁴ (Figure S2, Supplementary Information).

REFERENCES

1. Small, D. M., Dowling, R. H., and Redinger, R. N. (1972) The enterohepatic circulation of bile salts, *Arch. Intern. Med.* *130*, 552-573.
2. Borgström, B., Barrowman, J. A., and Lindström, M. (1985) Roles of bile acids in intestinal lipid digestion and absorption, in *Sterols and bile acids* (Danielsson, H., and Sjövall, J., Eds.), Vol. 12, pp 405-425, Elsevier, Amsterdam.
3. Makishima, M., Okamoto, A. Y., Repa, J. J., Tu, H., Learned, R. M., Luk, A., Hull, M. V., Lustig, K. D., Mangelsdorf, D. J., and Shan, B. (1999) Identification of a nuclear receptor for bile acids, *Science* *284*, 1362-1365.
4. Houten, S. M., Watanabe, M., and Auwerx, J. (2006) Endocrine functions of bile acids, *EMBO J* *25*, 1419-1425.
5. Banaszak, L., Winter, N., Xu, Z., Bernlohr D. A., Cowan, S., Jones, T. A. (1994) Lipid-binding proteins: a family of fatty acid and retinoid transport proteins, *Adv Protein Chem.*, *45*, 89-151.
6. Veerkamp, J. H., and Maatman, R. G. (1995) Cytoplasmic fatty acid-binding proteins: their structure and genes, *Prog. Lipid Res.* *34*, 17-52.
7. Tochtrup, G. P., Richter, K., Tang, C., Toner, J. J., Covey, D. F., and Cistola, D. P. (2002) Energetics by NMR: site-specific binding in a positively cooperative system, *Proc. Natl. Acad. Sci. U.S.A.* *99*, 1847-1852.
8. Turpin, E. R., Fang, H.-J., Thomas, N. R., and Hirst, J. D. (2013) Cooperativity and site selectivity in the ileal lipid binding protein, *Biochemistry*, *52*, 4723-4733.

9. Tochtrop, G. P., Bruns, J. M., Tang, C., Covey, D. F., and Cistola, D. P. (2003) Steroid ring hydroxylation patterns govern cooperativity in human bile acid binding protein, *Biochemistry* 42, 11561-11567.
10. Tochtrop, G. P., DeKoster, G. T., Covey, D. F., and Cistola, D. P. (2004) A single hydroxyl group governs ligand site selectivity in human ileal bile acid binding protein, *J. Am. Chem. Soc.* 126, 11024-11029.
11. Cogliati, C., Tomaselli, S., Assfalg, M., Pedo, M., Ferranti, P., Zetta, L., Molinari, H., and Ragona, L. (2009) Disulfide bridge regulates ligand-binding site selectivity in liver bile acid-binding proteins, *FEBS Journal* 276, 6011-6023.
12. Kurz, M., Brachvogel, V., Matter, H., Stengelin, S., Thüring, H., Kramer, W. (2003) Insights into the bile acid transportation system: the human ileal lipid-binding protein-cholyltaurine complex and its comparison with homologous structures, *Proteins*, 50, 312-328.
13. Lücke, C., Zhang, F., Rüterjans, H., Hamilton, J. A., and Sacchettini, J. C. (1996) Flexibility is a likely determinant of binding specificity in the case of ileal lipid binding protein, *Structure* 4, 785-800.
14. Horvath, G., Egyed, O., Bencsura, A., Simon, A., Tochtrop, G.P., DeKoster, G.T., Covey, D.F., Cistola, D.P., Toke, O., *personal communication*

15. Hodsdon, M. E., and Cistola, D. P. (1997) Ligand binding alters the backbone mobility of intestinal fatty acid-binding protein as monitored by ^{15}N NMR relaxation and ^1H exchange, *Biochemistry* 36, 2278-2290.
16. Cistola, D. P., Kim, K., Rogl, H., and Frieden, C. (1996) Fatty acid interactions with a helix-less variant of intestinal fatty acid-binding protein, *Biochemistry* 35, 7559-7565.
17. Lu, J., Cistola, D. P., and Li, E. (2003) Two homologous rat cellular retinol-binding proteins differ in local conformational flexibility, *J. Mol. Biol.* 330, 799-812.
18. Horváth, G., Király, P., Tárkányi, G., and Toke, O. (2012) Internal motions and exchange processes in human ileal bile acid binding protein as studied by backbone ^{15}N nuclear magnetic resonance spectroscopy, *Biochemistry* 51, 1848-1861, with *erratum* in *Biochemistry* 51, 10119 (2012).
19. Ragona, L., Catalano, M., Luppi, M., Cicero, D., Eliseo, T., Foote, J., Fogolari, F., Zetta, L., and Molinari, H. (2006) NMR dynamic studies suggest that allosteric activation regulates ligand binding in chicken liver bile acid-binding protein, *J. Biol. Chem.* 281, 9697-9709.
20. Sacchettini JC, Gordon JI, Banaszak LJ (1989) Crystal Structure of rat intestinal fatty-acid-binding protein. Refinement and analysis of the Escherichia coli-derived protein with bound palmitate. *J. Mol. Biol.* 208, 327–339.
21. Friedman, R., Nachliel, E., and Gutman, M. (2005) Molecular dynamics simulations of the adipocyte lipid binding protein reveal a novel entry site for the ligand, *Biochemistry* 44, 4275-4283.

22. Ragona, L., Pagano, K., Tomaselli, S., Favretto, F., Ceccon, A., Zanzoni, S., D'Onofrio, M., Assfalg, M., and Molinari, H. (2014) The role of dynamics in modulating ligand exchange in intracellular lipid binding proteins. *Biochim. Biophys. Acta – Proteins and Proteomics* **1844**, 1268-1278.
23. Toke, O., Monsey, J. D., DeKoster, G. T., Tochtrop, G. P., Tang, C., and Cistola, D. P. (2006) Determinants of cooperativity and site-selectivity in human ileal bile acid-binding protein, *Biochemistry* **45**, 727-737.
24. Toke, O., Monsey, J. D., and Cistola, D. P. (2007) Kinetic mechanism of ligand binding in human ileal bile acid binding protein as determined by stopped-flow fluorescence analysis, *Biochemistry* **46**, 5427-5436.
25. Wittekind, M., and Mueller, L. (1993) HNCACB, a high sensitivity 3D NMR experiment to correlate amide-proton and nitrogen resonances with the alpha- and beta-carbon resonances in proteins, *J. Magn. Res. B* **101**, 201-205.
26. Muhindaram, D. R., and Kay, L. E. (1994) Gradient-enhanced triple-resonance three-dimensional NMR experiments with improved sensitivity, *J. Magn. Res. B*, **103**, 203-216.
27. Kay, L. E., Xu, G. Y., and Yamazaki, T. (1994) Enhanced-sensitivity triple-resonance spectroscopy with minimal H₂O saturation, *J. Magn. Res. A* **109**, 129-133.
28. Grzesiek, S., and Bax, A. (1992) Correlating backbone amide and side chain resonances in larger proteins by multiple relayed triple resonance NMR, *J. Am. Chem. Soc.* **114**, 6291-6293.

29. Kay, L. E., Keifer, P., and Saarinen, T. (1992) Pure absorption gradient enhanced heteronuclear single quantum correlation spectroscopy with improved sensitivity, *J. Am. Chem. Soc.* 114, 10663-10665.
30. Kay, L., Nicholson, L., Delaglio, F., Bax, A., and Torchia, D. (1992) Pulse sequences for removal of the effects of cross-correlation between dipolar and chemical-shift anisotropy relaxation mechanism on the measurement of heteronuclear T1 and T2 values in proteins, *J. Magn. Res.* 97, 359-375.
31. Farrow, N. A., Muhandiram, R., Singer, A. U., Pascal, S. M., Kay, C. M., Gish, G., Shoelson, S. E., Pawson, T., Forman-Kay, J. D., and Kay, L. E. (1994) Backbone dynamics of a free and phosphopeptide-complexed Src homology 2 domain studied by ¹⁵N NMR relaxation, *Biochemistry* 33, 5984-6003.
32. Markley, J. L., Horsley, W. J., and Klein, M. P. (1971) Spin-lattice relaxation measurements in slowly relaxing complex spectra, *J. Chem. Phys.* 55, 3604-3605.
33. Loria, J. P., Rance, M., Palmer, A. G. III (1999) A relaxation-compensated Carr-Purcell-Meiboom-Gill sequence for characterizing chemical exchange by NMR spectroscopy, *J. Am. Chem. Soc.* 121, 2331-2332.
34. Tollinger, M., Skrynnikov, N. R., Mulder, F. A. A., Forman-Kay, J. D., and Kay, L. E. (2001) Slow dynamics of folded and unfolded states of an SH3 domain, *J. Am. Chem. Soc.*, 123, 11341-11352.
35. Mulder, F. A., Skrynnikov, N. R., Hon, B., Dahlquist, F. W., and Kay, L. E. (2001) Measurement of slow (micros-ms) time scale dynamics in protein side chains by (15)N

relaxation dispersion NMR spectroscopy: application to Asn and Gln residues in a cavity mutant of T4 lysozyme, *J. Am. Chem. Soc.* 123, 967-975.

36. Abragam, A. (1961) *Principles of Nuclear Magnetism*, Clarendon Press, Oxford.
37. Case, D. A. (1999) Calculations of NMR dipolar coupling strengths in model peptides, *J. Biomol. NMR* 15, 95-102.
38. Lipari, G., and Szabo, A. (1982) Model-free approach to the interpretation of nuclear magnetic resonance relaxation in macromolecules. 1. Theory and range of validity, *J. Am. Chem. Soc.* 104, 4546-4559.
39. Lipari, G., and Szabo, A. (1982) Model-free approach to the interpretation of nuclear magnetic resonance relaxation in macromolecules. 2. Analysis of experimental results, *J. Am. Chem. Soc.* 104, 4559-4570.
40. Clore, G. M., Driscoll, P. C., Wingfield, P. T., and Gronenborn, A. M. (1990) Analysis of backbone dynamics of interleukin-1 β using two-dimensional inverse detected heteronuclear ^{15}N - ^1H NMR spectroscopy, *Biochemistry* 29, 7387-7401.
41. Clore, G. M., Szabo, A., Bax, A., Kay, L. E., Driscoll, P. C. and Gronenborn, A. M. (1990) Deviations from the simple two-parameter model free approach to the interpretation of ^{15}N nuclear magnetic relaxation of proteins, *J. Am. Chem. Soc.* 112, 4989-4991.
42. Cole, R., and Loria, J. P. (2003) FAST-Modelfree: A program for rapid automated analysis of solution NMR spin-relaxation data, *J. Biomol. NMR*, 26, 203-213.

43. Mandel, A. M., Akke, M., and Palmer, A. G. (1995) Backbone dynamics of *Escherichia coli* ribonuclease HI: Correlations with structure and function in an active enzyme, *J. Mol. Biol.* 246, 144-163.
44. Palmer, A. G., Rance, M., and Wright, P. E. (1991) Intramolecular motions of a zinc finger DNA-binding domain from xfin characterized by proton-detected natural abundance ^{13}C heteronuclear NMR spectroscopy, *J. Am. Chem. Soc.* 113, 4371-4380.
45. Kay, L. E., Torchia, D. A., and Bax, A. (1989) Backbone dynamics of proteins as studied by ^{15}N inverse detected heteronuclear NMR spectroscopy: Application to *Staphylococcal nuclease*, *Biochemistry* 28, 8972-8979.
46. Li, Z., Raychaudhuri, S., and Wand, A. J. (1996) Insights into the local residual entropy of proteins provided by NMR relaxation, *Protein Sci.* 5, 2647-2650.
47. Yang, D., and Kay, L. E. (1996) Contributions to conformational entropy arising from bond vector fluctuations measured from NMR-derived order parameters: application to protein folding, *J. Mol. Biol.* 263, 369-382.
48. Korzhnev, D. M., Kloiber, K., and Kay, L. E. (2004) Multiple-quantum relaxation dispersion NMR spectroscopy probing millisecond time-scale dynamics in proteins: theory and application, *J. Am. Chem. Soc.* 126, 7320-7329.
49. Kleckner, I. R., and Foster, M. P. (2012) GUARDD: user-friendly MATLAB software for rigorous analysis of CPMG RD NMR data, *J. Biomol. NMR* 52, 11-22.
50. Forman-Kay, J.D. (1999) The ‘dynamics’ in the thermodynamics of binding, *Nat. Struct. Biol.* 6, 1086–1087.

51. Cogliati, C., Ragona, L., D'Onofrio, M., Günther, U., Whittaker, S., Ludwig, C., Tomaselli, S., Assfalg, M., and Molinari, H. (2010) Site-specific investigation of the steady-state kinetics and dynamics of the multistep binding of bile acid molecules to a lipid carrier protein, *Chem. Eur. J.* **16**, 11300-11310.
52. Zanzoni, S., Assfalg, M., Giorgetti, A., D'Onofrio, M., and Molinari, H. (2011) Structural requirements for cooperativity in ileal bile acid-binding proteins, *J. Biol. Chem.* **286**, 39307-39317.
53. Vinther, J. M., Kristensen, S. M., and Led, J. J. (2011) Enhanced stability of a protein with increasing temperature, *J. Am. Chem. Soc.* **133**, 271-278.
54. Pistolesi, S., and Tjandra N. (2012) Temperature dependence of molecular interactions involved in defining stability of glutamine binding protein and its complex with L-glutamine, *Biochemistry* **51**, 643-652.
55. Akke, M., Brüschweiler, R., and Palmer, A. G. (1993) NMR order parameters and free energy: An analytical approach and its application to cooperative Ca^{2+} binding by calbindin D_{9k}, *J. Am. Chem. Soc.* **115**, 9832-9833.
56. Creamer, T. P., and Rose, G. D. (1992) Side-chain entropy opposes alpha-helix formation but rationalizes experimentally determined helix-forming propensities, *Proc. Natl. Acad. Sci. U.S.A.* **89**, 5937-5941.
57. Pickett, S. D., and Sternberg, M. J. E. (1993) Empirical scale of side-chain conformational entropy in protein folding, *J. Mol. Biol.* **231**, 825-839.

58. Spolar, R. S., and Record, M. T. (1994) Coupling of local folding to site-specific binding of proteins to DNA, *Science*, *263*, 777-784.
59. Privalov, P. L., and Makhatadze, G. I. (1993) Contribution of hydration to protein folding thermodynamics. II. The entropy and Gibbs energy of hydration. *J. Mol. Biol.* *232*, 660-679.
60. Makhatadze, G. I., and Privalov, P. L. (1995) Energetics of protein structure, *Adv. Protein Chem.* *47*, 307-425.
61. Dubins, D. N., Filfil, R., Macgregor, R. B. Jr., and Chalikian, T. V. (2000) Volume and compressibility changes accompanying thermally-induced native-to-unfolded and molten globule-to-unfolded transitions of cytochrome c: a high pressure study. *J. Phys. Chem. B* *104*, 390-401.
62. Némethy, G., and Scheraga, H.A. (1962) Structure of water and hydrophobic bonding in proteins. I. The thermodynamic properties of hydrophobic bonds in proteins, *J. Phys. Chem.* *66*, 1773-1789.
63. Baldwin, R. L. (1986) Temperature dependence of the hydrophobic interaction in protein folding, *Proc. Natl. Acad. Sci. U.S.A.*, *83*, 8069–8072.

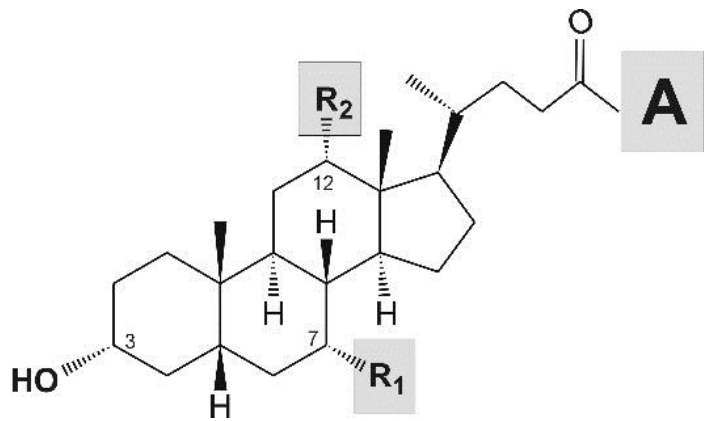


Fig. 1

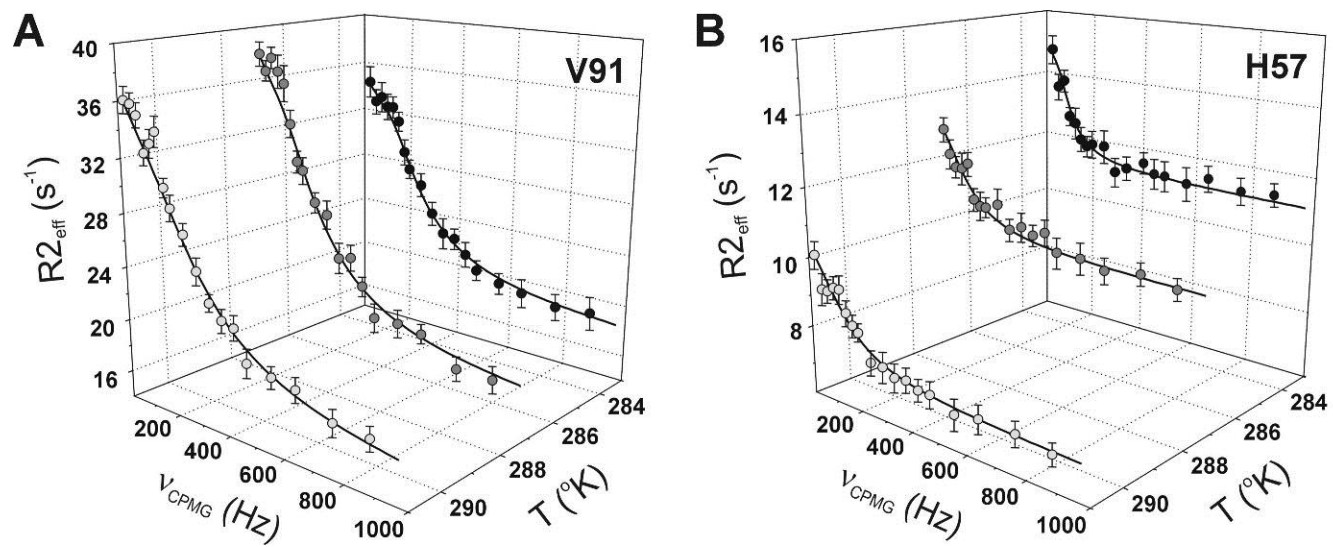


Fig. 2

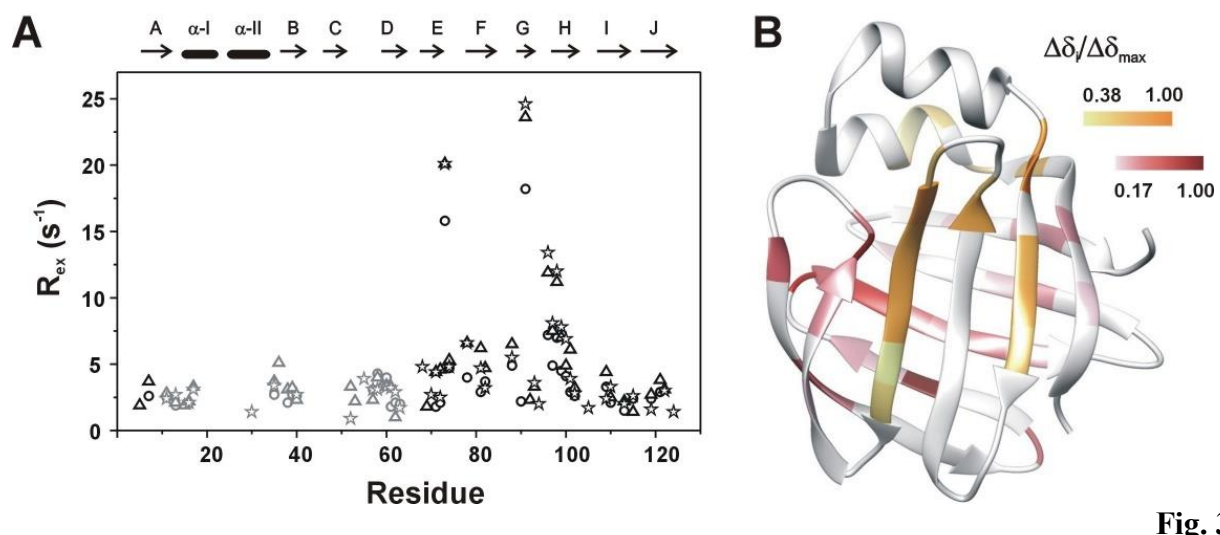


Fig. 3

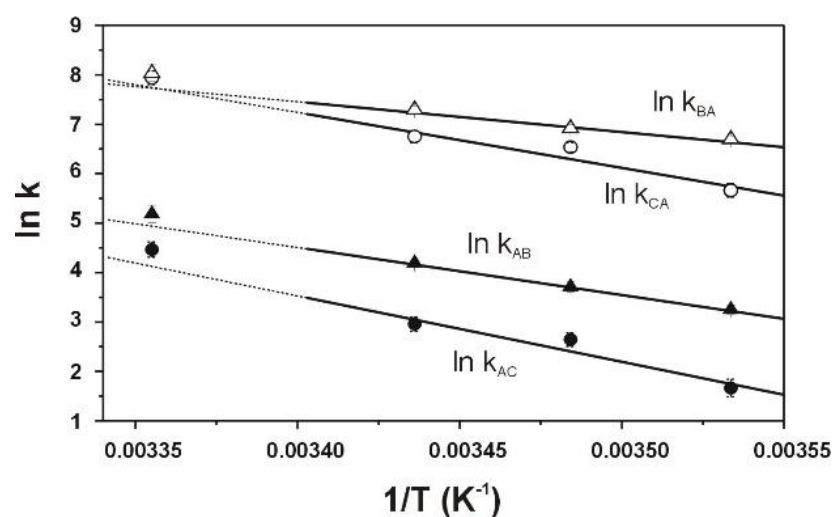


Fig. 4

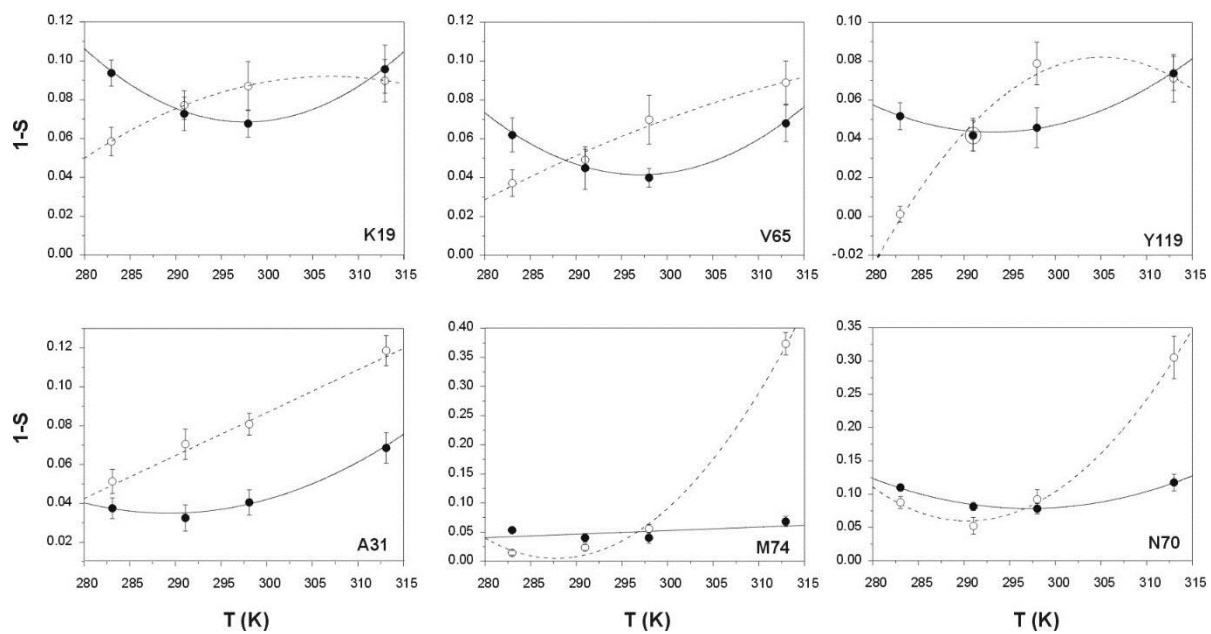


Fig. 5

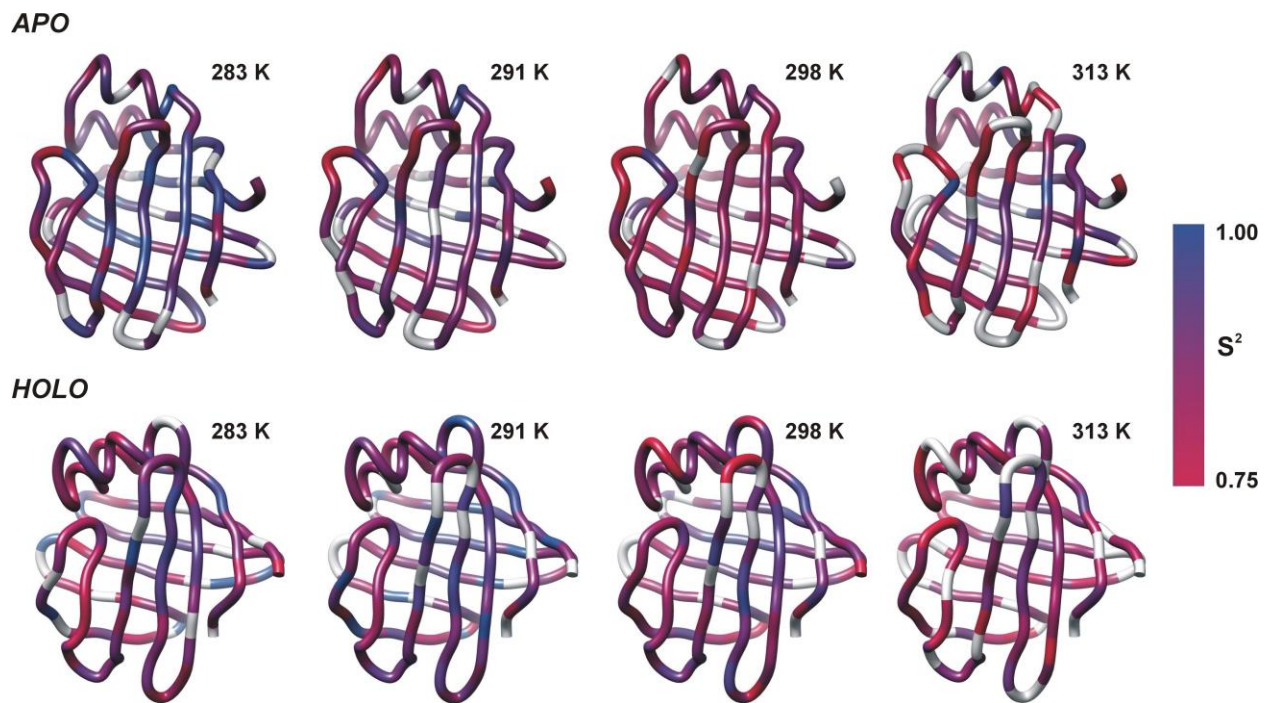


Fig. 6

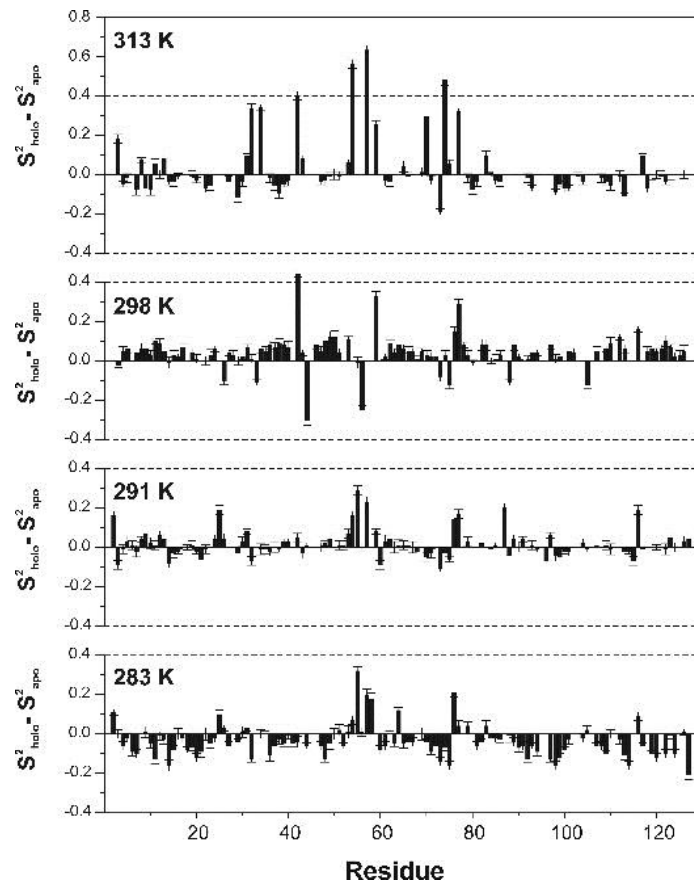


Fig. 7

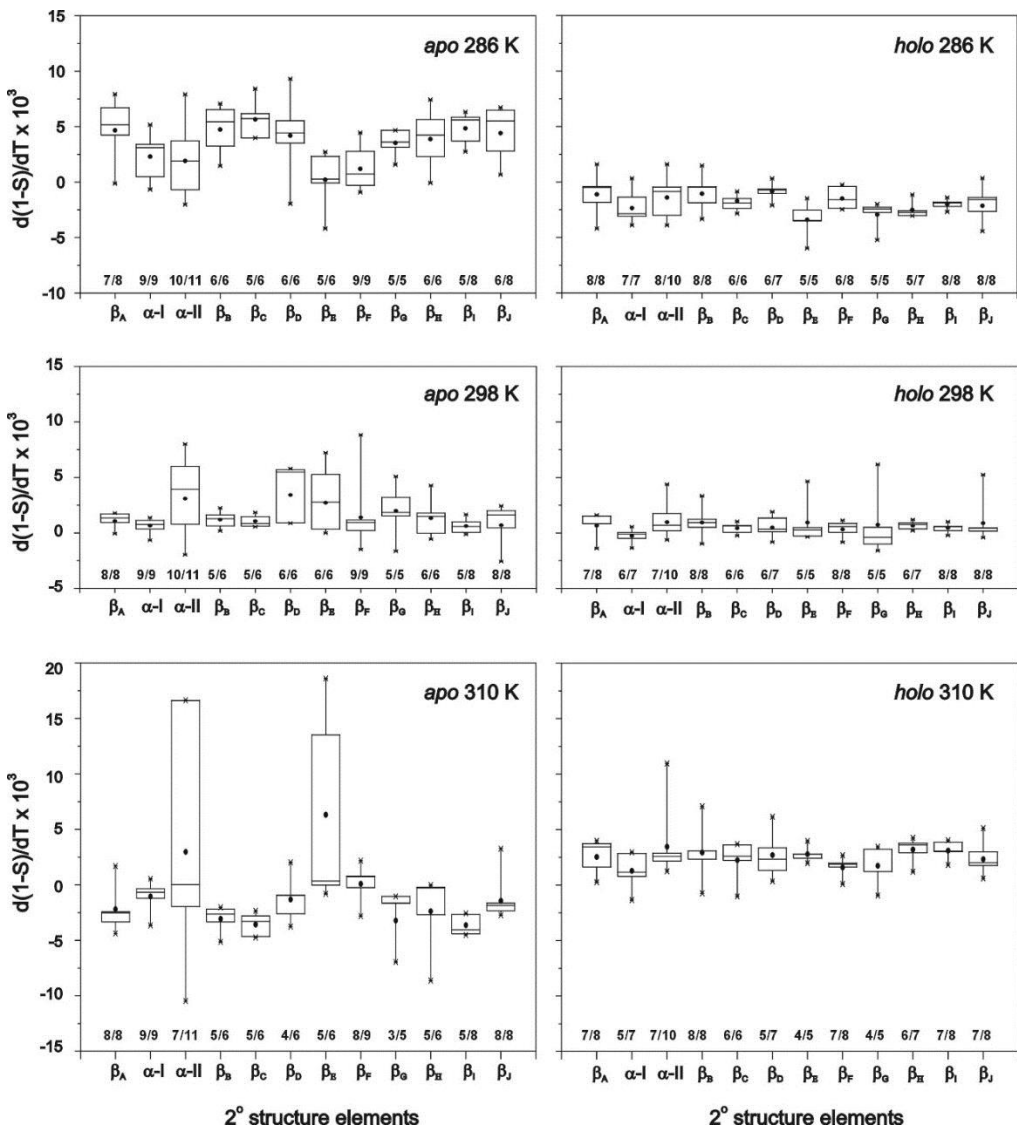


Fig. 8

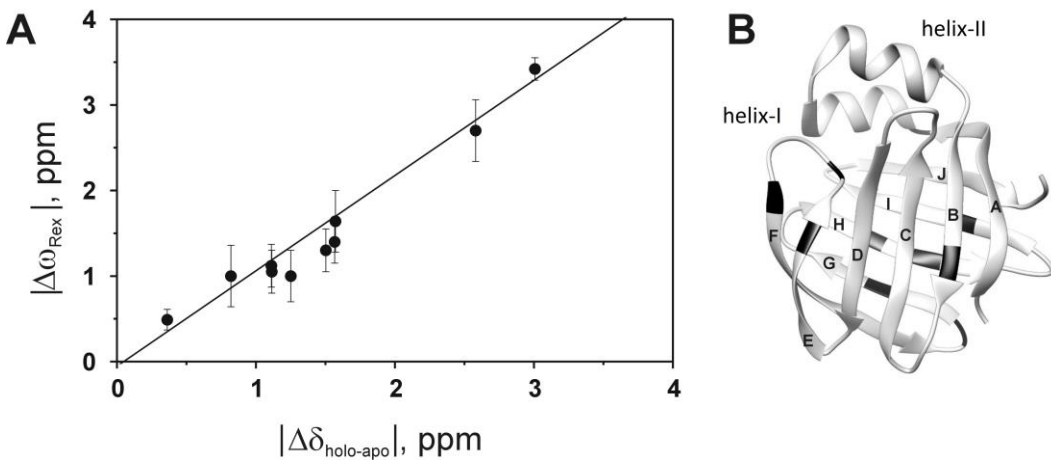


Fig. 9

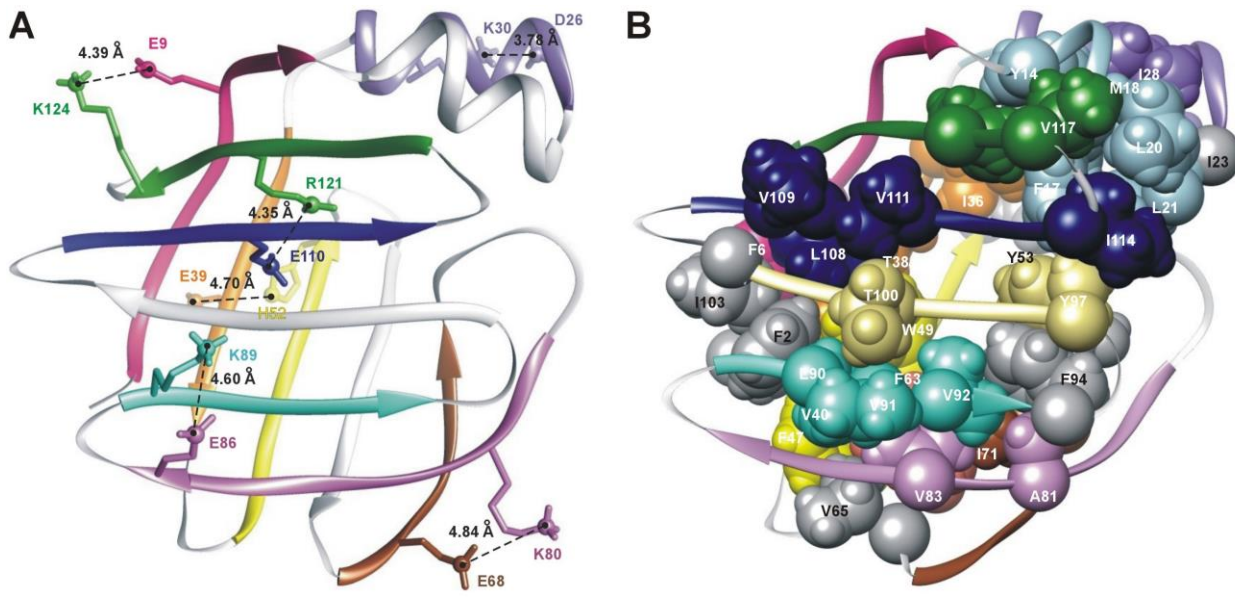
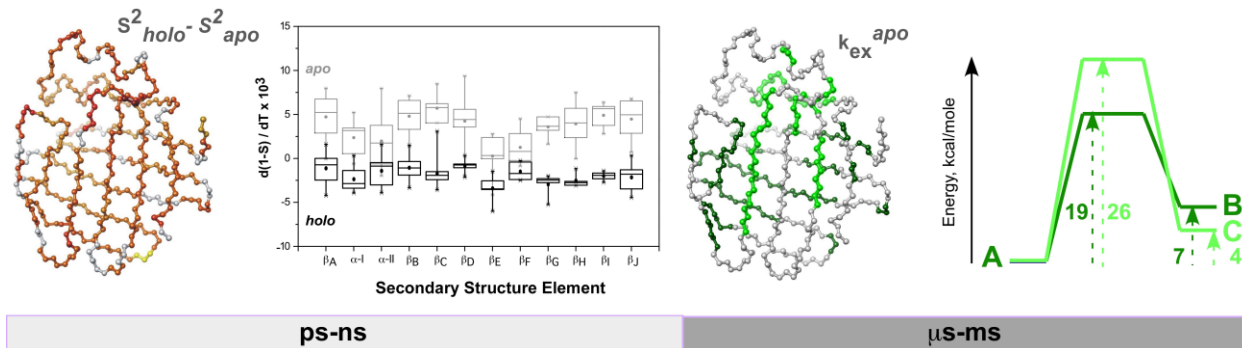


Fig. 10

For Table of Contents Use Only



Temperature Dependence of Backbone Dynamics in Human Ileal Bile Acid-Binding Protein.

Implications for the Mechanism of Ligand Binding

Gergő Horváth, Orsolya Egyed, and Orsolya Toke